Eclogitisation of dry and impermeable granulite by fluid flow with reaction-induced porosity: insights from hydro-chemical modelling

Erwan Bras, Philippe Yamato, Stefan M Schmalholz, Thibault Duretz, Yury Y Podladchikov

Eclogitisation of dry and impermeable granulite by fluid flow with reaction-induced porosity: insights from hydro-chemical modelling

Erwan Bras[a,*], Philippe Yamato[a,b], Stefan M. Schmalholz[c], Thibault Duretz[d], Yury Y. Podladchikov[c,e]

[a] *Univ. Rennes, CNRS, Géosciences Rennes UMR 6118, 35000 Rennes, France*
[b] *Institut Universitaire de France, 75005 Paris, France*
[c] *Institute of Earth Sciences, University of Lausanne, 1015 Lausanne, Switzerland*
[d] *Institut für Geowissenschaften, Goethe-Universität Frankfurt, Frankfurt, Germany*
[e] *Faculty of Mechanics and Mathematics, Lomonosov Moscow State University, Moscow, Russia*

Abstract

Eclogitisation is a major metamorphic process of continental subduction zones, where transformation of dry lower crustal rocks into eclogites seem to correlate with seismogenic events. Eclogitisation can occur at high pressure during hydration of granulite, but the physical processes controlling the hydration of dry, impermeable granulite remain poorly understood. Here, we present a new fully coupled hydro-chemical model of a non-deforming porous rock which undergoes metamorphic reactions in response to fluid pressure variations. Conservation equations for total and solid mass are solved, and fluid and solid densities are calculated with look-up tables computed from models relying on equilibrium thermodynamics. Our model shows that a fluid pressure pulse generates a pressure gradient that causes densification when the pressure required for eclogitisation is reached. The reaction generates porosity and subsequent porous fluid flow into the initially non-porous impermeable granulite. This process lasts as long as the pressure pulse is maintained, but high pressure within eclogite can persist for a longer time. The hydration front propagates tens of centimetres into the granulite in the order of weeks to months. We show that propagation of a hydration-reaction front is effectively a diffusive process, with diffusivity in the order of 10^{-9} $m^2 \cdot s^{-1}$ for eclogitisation as in Holsnøy, Norway. Reactive hydration of impermeable granulite is possible because its solid density is smaller than that of eclogite. We discuss the application of our model for eclogitisation and also for other reactions for which hydration of impermeable rock is possible.

Keywords: Eclogitization, hydration front, reaction-induced porosity, hydro-chemical modelling

*Corresponding author

1. Introduction

The physical properties of the continental crust, such as density, viscosity and permeability, critically affect fluid migration, orogenic cycles and seismicity, and are primarily controlled by the metamorphic state of the lower crust (Austrheim, 1998; Jackson et al., 2004). Eclogitisation of dry and mechanically strong crustal rocks involves a large increase in solid density, transient rheological weakening, and fluid flow (e.g. Austrheim, 1987; Bras et al., 2021), which play a major role for the stress state of the crust, seismicity and long-term lithosphere dynamics (Labrousse et al., 2010; Jamtveit et al., 2018a; Yamato et al., 2019; Moulas et al., 2022). For example, the strong feedbacks between metamorphism, deformation, and fluid transport in the lower crust (John and Schenk, 2006; Austrheim, 2013; Jamtveit et al., 2019) are crucial for determining the physical mechanisms that initiate earthquakes (Miller, 2013; Menegon et al., 2021). Hence, studying eclogitisation of dry crustal rocks is crucial for our understanding of the properties and dynamics of the deep crust (Jamtveit et al., 2019).

The interplay between metamorphism, deformation, and fluid flow can be inferred through geophysical investigations in active orogens (e.g. in the Himalaya, Hetényi et al., 2007), high pressure laboratory rock deformation experiments (Incel et al., 2017; Shi et al., 2018) and mathematical modelling based on the concepts of continuum mechanics and thermodynamics (Malvoisin et al., 2020; Schmalholz et al., 2020; Moulas et al., 2022; Yamato et al., 2022). However, investigating this interplay with direct petrological and structural observations from exhumed crustal rocks in the field is essential to understand how metamorphic reactions control the properties of the deep crust (Jackson et al., 2004; Labrousse et al., 2010; Baïsset et al., 2023).

The island of Holsnøy, in southwestern Norway, constitutes an ideal natural laboratory for investigating the interplay between metamorphism, deformation and fluid flow in the lower crust (Austrheim, 1987, 2013; Putnis et al., 2017). A large part of the island is made of anorthositic granulites, which were formed at ca. 930 Ma during the Grenvillian orogeny (Bingen et al., 2001). During the Caledonian orogeny, the granulites were subducted during convergence and collision between Baltica and Laurentia (Andersen et al., 1991). The high-pressure event occurring during the collision stage caused the partial eclogitisation of the granulitic lower crust, associated with fluid infiltration and shear deformation, and was presumably initiated by fracturing associated with earthquakes (Austrheim, 1987). Peak pressure (P) and temperature (T) conditions in Holsnøy were 670-690 °C and 21-22 kbar (Bhowany et al., 2018). The relation between eclogite and granulite is exceptionally well preserved, making Holsnøy an ideal analogue for the metamorphic state of the lower crust being deeply buried during orogenic events (Jackson et al., 2004; Labrousse et al., 2010).

In Holsnøy, eclogitisation is spatially heterogeneous at the outcrop scale and is localised in eclogite shear zones crosscutting the granulite protolith, and in eclogite fingers overprinting the granulite without associated deformation (Zertani et al., 2019; Kaatz et al., 2021; Putnis et al., 2021). Our study concerns both eclogite shear zones and eclogite fingers (see examples in figure 1), which will

both be referred to as "eclogitisation zones" in the rest of this study.

Several authors (e.g. Austrheim, 1987; Zertani et al., 2022; Kaatz et al., 2022) argued that eclogite and granulite coexist in close spatial proximity in eclogitisation zones because granulite is metastable: granulite experienced eclogite facies $P-T$ conditions, but remained largely untransformed because it lacked fluids to trigger eclogitisation. Only regions infiltrated by fluids transformed into eclogite. However, recent studies suggested that the coexistence of granulite and eclogite due to local pressure variations may be a more consistent interpretation of the field data (Putnis et al., 2021 and references therein). Here, we do not aim to demonstrate which interpretation is more feasible, because our study is compatible with both interpretations.

Several studies suggest that eclogitisation zones widen over time (Jamtveit et al., 2000; Jolivet et al., 2005; Bras et al., 2021; Kaatz et al., 2021), but existing numerical models do not explain this widening with consistent physics, coupling metamorphic reaction and fluid flow. For example, Jamtveit et al. (2000) explain the development of static eclogitisation zones with a model coupling solid state diffusion and generation of a network of fractures in an elastic model, without porous fluid flow. Bras et al. (2021) and Kaatz et al. (2021) model the widening of eclogitisation zones with a diffusion equation which mimics the effects of porous fluid flow and/or solid state diffusion of hydrogen and oxygen. Moulas et al. (2022) present a purely mechanical model for metamorphism of the lower crust, without any hydro-chemical aspect, to study the long-term (order of millions of years) impact of such metamorphism on crustal dynamics. Malvoisin et al. (2020) consider porous fluid flow with a fully coupled hydro-chemical-mechanical model and show that hydration of dry granulite can occur in the order of weeks. However, they focus on the influence of the reaction on the generation of seismicity but not on the mechanism of widening of eclogitisation zones. Therefore, although several models already describe the eclogitisation of granulite, it is still not clear how to predict the evolution of eclogitisation zones based on theoretical models which couple reactions and porous fluid flow.

Here, we investigate the time evolution of eclogitisation driven by porous fluid flow following Darcy's law. We apply a simple but physically consistent one dimensional (1D) hydro-chemical (HC) model involving metamorphic reactions, based on the concepts of continuum mechanics and local equilibrium thermodynamics, similar to models presented by Malvoisin et al. (2015), Plümper et al. (2017), and Schmalholz et al. (2020). Pressure variations modify the rock density by solid compressibility and by replacement of low-density granulite-facies minerals with high density eclogite-facies minerals. Density changes that decrease the rock volume generate porosity, and hence permeability if it is dependent on porosity. Permeability associated with fluid pressure gradients leads to fluid flow and reaction front propagation. Our aims are to (1) quantify the widening of the eclogitisation zones and (2) explain the mechanism of hydration of a zero-porosity, and thus impermeable, granulite by porous fluid flow.

From a technical point of view, modelling fluid flow into a zero-porosity region is indeed challenging.

The zero porosity limit is typically met in studies involving two-phase flow (e.g. Scott and Stevenson, 1986). Although the set of governing two-phase equations reduce to single-phase equations in the zero porosity limit (e.g. Katz et al., 2007), accounting for transient variations of the relative proportion of porous and non-porous domains in a single simulation can be challenging. Several studies get around this problem by having a minimal background porosity in the dry phases (e.g. Räss et al., 2019; Schmalholz et al., 2020), which allows to apply two-phase flow equations to the whole domain. Other authors have addressed this problem by including a specific treatment of these equations (e.g. Arbogast et al., 2017). In this paper we also address this issue in the context of the hydration of a zero-porosity region.

With our model, we show that fluid flow induced hydration and subsequent eclogitisation of a dry and impermeable rock is possible. We explain the physical mechanisms by which the eclogitisation zones can widen into an initially zero-porosity region, and provide a numerical tool allowing to simulate this process.

2. Methods

We consider a 1D hydro-chemical (HC) model, similar to that of Plümper et al. (2017), where a non-deforming porous rock undergoes metamorphic reactions in response to fluid pressure variations. The model is based on local thermodynamic equilibrium and mass conservation. Metamorphic reactions lead to changes in rock density and exchange of H_2O between the fluid and the solid, hence modifying the porosity of the system. Since we use a porosity-dependant, Carman-Kozeny type permeability (Costa, 2006), changes in porosity also modify the permeability. Reaction-induced permeability leads to fluid flow controlled by fluid pressure gradients.

2.1. Governing system of equations

In our model, the volatile species, assumed here to be pure H_2O, are either structurally bound to the solid, having a particular solid mass fraction X_{H_2O}, or constitute the fluid filling the porosity. We assume that dissolution of solid species, such as Si, Al, Na and Ca, in the fluid is negligible. Following Malvoisin et al. (2015); Plümper et al. (2017); Schmalholz et al. (2020), solving this system requires (1) conservation of total mass per unit volume of the system (ρ_T, i.e. sum of fluid mass and solid mass) and (2) conservation of the mass per unit volume of solid species (ρ_T^s). All variables used in this study are listed in table 1.

2.1.1. Conservation of total mass

We consider a porous medium, with porosity ϕ, which consists of a solid phase with density ρ_s and a fluid phase with density ρ_f stored in the pores. Per unit volume, the total mass ρ_T of the porous medium is:

$$\rho_T = \rho_f \phi + \rho_s (1 - \phi). \tag{1}$$

In a general case, the one-dimensional conservation equation of a given quantity A, expressing the variation of quantity A (per unit volume) over time, is:

$$\frac{\partial A}{\partial t} = -\frac{\partial q_A}{\partial x}. \tag{2}$$

In absence of diffusive flux, the flux of A (q_A) is purely advective and can be expressed as:

$$q_A = A v_A, \tag{3}$$

which is simply the amount of A multiplied by the velocity of A. Using equations (1) and (3), the advective flux of total mass ρ_T can be written as:

$$q_{\rho_T} = \rho_f \phi v_f + \rho_s (1-\phi) v_s, \tag{4}$$

where v_f and v_s are respectively the velocities of the fluid and the solid. Using equations (2) and (4), the conservation of total mass ρ_T is then:

$$\frac{\partial \rho_T}{\partial t} = -\frac{\partial}{\partial x}(\rho_f \phi v_f + \rho_s (1-\phi) v_s). \tag{5}$$

In the absence of solid deformation ($v_s = 0$), the conservation equation of total mass simplifies to:

$$\frac{\partial \rho_T}{\partial t} = -\frac{\partial}{\partial x}(\rho_f \phi v_f). \tag{6}$$

The force balance for the fluid in the absence of gravity and solid velocity can be expressed using Darcy's law:

$$\phi v_f = -\frac{k_0 \phi^3}{\eta_f}\left(\frac{\partial P_f}{\partial x}\right), \tag{7}$$

where k_0 is the permeability coefficient in a porosity-dependant Carman-Kozeny type permeability expression, η_f is the fluid viscosity, and P_f is the fluid pressure. Substituting equation (7) into equation (6) yields the total mass conservation equation:

$$\frac{\partial \rho_T}{\partial t} = \frac{\partial}{\partial x}\left[\rho_f \frac{k \phi^3}{\eta_f}\left(\frac{\partial P_f}{\partial x}\right)\right]. \tag{8}$$

2.1.2. Total solid mass

We assume that solid components, such as Si, Al, Na and Ca, never enter the fluid phase, whereas the volatile component H_2O can be part of the solid phase in the form of hydrous minerals. X_{H_2O} is the mass fraction of volatile components structurally bound in the solid. The total solid mass (without structurally bound H_2O) of the system per unit volume, ρ_T^s, is:

$$\rho_T^s = \rho_s (1-\phi)(1 - X_{H_2O}). \tag{9}$$

Solid components remain in the solid, so in the absence of solid velocity there is never any advective flux of solid mass (equation 3), and thus there is no time evolution of ρ_T^s:

$$\frac{\partial \rho_T^s}{\partial t} = 0. \tag{10}$$

Hence, equation (9) can be used to express the solid mass conservation equation if ρ_T^s is a known, constant parameter of the model.

2.2. Precomputed thermodynamic data

2.2.1. Thermodynamic model

The equations described above require prior knowledge of the densities of fluid, eclogite and granulite at any pressure, as well as the amount of fluid structurally bound to the solid X_{H_2O}. We compute these values by minimisation of Gibbs free-energy using the software Perple_X (Connolly, 2005), with the internally consistent thermodynamic data set of Holland and Powell (1998).

To study the eclogitisation of granulite in Holsnøy, we consider the model chemical system Na_2O-CaO-SiO_2-Al_2O_3-H_2O. We do not consider FeO and MgO because the main reactions of granulite to eclogite are destabilisation of the anorthite and albite components of plagioclase (e.g. Bras et al., 2021): with increasing pressure and in the presence of water, anorthite transforms into zoisite, kyanite and quartz, and albite transforms into jadeite and quartz. Our modelled granulite is therefore composed of only plagioclase, and our modelled eclogite of jadeite, zoisite, kyanite, quartz. We use a system composition of 57.64 wt% SiO_2, 26.92 wt% Al_2O_3, 8.76 wt% CaO and 6.68 wt% Na_2O, without FeO or MgO, corresponding to a representative composition of plagioclase in Holsnøy granulite (Bras et al., 2021). We use the solid solution for plagioclase of Newton et al. (1980) (Pl(h) in Perple_X). We use a constant bulk composition and variable water content, as there is no major variation of composition between granulite and eclogite, besides the introduction of water (Centrella, 2019; Bras et al., 2021). Rock properties are computed at a constant temperature of 700°C, consistent with temperature estimates in both granulite and eclogite by Bhowany et al. (2018).

The aim of the thermodynamic calculation is to compute bulk rock densities as a function of pressure in order to use them in our model, and not to predict mineral assemblages. We can therefore simplify the thermodynamic database by only including minerals that are present in substantial proportions in Holsnøy granulites and eclogites. This simplification produces the pseudosection displayed in figure 2A. With this simplified set-up, dry granulite is modelled with pure plagioclase and no water at low pressure, and hydrous eclogite is modelled with the products of plagioclase destabilisation (jadeite + kyanite + zoisite + quartz) and water at high pressure (figure 2A, yellow line). Due to the aforementioned simplifications the modelled data is not identical to field data, but has the same general behaviour: a jump in density and amount of fluid stored in minerals between granulite and eclogite.

When solid-fluid interactions are considered, it is the fluid pressure that determines which phases are stable in a local equilibrium domain, rather than the mean stress (e.g Dahlen, 1992). Indeed, Llana-Fúnez et al. (2012) experimentally demonstrated that metamorphic reactions are controlled by fluid pressure rather than by confining pressure. Fluid pressure is therefore an appropriate macroscopic proxy of the pressure rocks are in equilibrium with, but in the absence of porosity there is no fluid pressure. Hence, throughout this study we use the general term "pressure" (P) to designate both fluid pressure in porous rocks and mean stress in rocks without porosity.

2.2.2. Look-up tables

The solid density ρ_s, fluid density ρ_f, and the amount of fluid structurally bound in the solid X_{H_2O} at each pressure are precomputed with the thermodynamic model described above, for use as look-up tables during simulations:

$$\rho_s = \rho_s(P), \tag{11a}$$

$$\rho_f = \rho_f(P), \tag{11b}$$

$$X_{H_2O} = X_{H_2O}(P). \tag{11c}$$

Additionally, an inverse look-up table can be computed using these data. At any given pressure, the values of ρ_s, ρ_f and X_{H_2O} are thermodynamically constrained (equation 11). Since the value of ρ_T^s is a known parameter of the model, ϕ can be computed at any pressure as well, using equation (9). ϕ, ρ_s and ρ_f can then be used to compute ρ_T with equation (1), ending up with a total mass look-up table ($\rho_T = \rho_T(P)$, figure 2B). ρ_T must monotonously increase with pressure, which is a consequence of thermodynamic stability (e.g. Landau and Lifshitz, 1980). Hence, for every given pressure there is a uniquely corresponding ρ_T. This uniqueness makes the inverse statement true: for every given ρ_T there is one uniquely corresponding pressure. We therefore have an inverse look-up table of the form:

$$P = P(\rho_T). \tag{12}$$

This inverse look-up table approach allows our model to account for both porous and non-porous regions. There is thus no need to assume an artificially low porosity in the non-porous domain.

2.3. Solving procedure

All partial differential equations are approximated with a finite-difference discretisation (e.g. Gerya, 2019). Our HC model consists of a closed system of 6 unknowns (ρ_s, ρ_f, X_{H_2O}, ρ_T, ϕ, P) and 6 equations (8, 9, 11a, 11b, 11c, 12). We use a pseudo-transient method (e.g. Räss et al., 2022) to iteratively solve these 6 equations until a converged solution is found, proceeding as follows:

1. Use the forward look-up tables (equation 11) to compute ρ_s, ρ_f and X_{H_2O} as a function of P,
2. Rearrange equation (9) to solve for ϕ as a function of ρ_s and X_{H_2O}:

$$\phi = 1 - \frac{\rho_T^s}{\rho_s(1 - X_{H_2O})}, \tag{13}$$

3. Explicitly solve equation (8) to compute ρ_T as a function of ϕ, P and ρ_f:

$$\rho_T^{new} = \rho_T^{old} + \frac{\partial}{\partial x}\left[\rho_f \frac{k\phi^3}{\eta_f}\left(\frac{\partial P}{\partial x}\right)\right] \times dt, \tag{14}$$

4. Use the inverse look-up table (equation 12) to compute P as a function of ρ_T.

In practice, at each time step we iterate this set of equations until the difference in calculated pressure from one iteration to another is smaller than a chosen convergence tolerance.

2.4. Model configuration

The parameters of our reference model are chosen to be close to natural values reported in the literature. Unless stated otherwise, all simulations displayed in this study use the parameters described below and shown in table 1.

2.4.1. Starting conditions

A common explanation of the development of eclogitisation zones (e.g. Austrheim, 1987; Zertani et al., 2019; Kaatz et al., 2021) can be summarised as follows: (1) Lower crustal earthquakes cause stress pulses and propagate fractures in the brittle granulite, which act as a pathway for fluids. (2) Fluid availability triggers eclogitisation. (3) Infiltration of fluid into the granulite further promotes eclogitisation. Our model reproduces this configuration (figure 3): when the simulation starts, the entire domain is made up of granulite, with pressure set at $P_{\mathrm{bg}} = 15$ kbar, close to the pressure of seismic faulting reported by Bhowany et al. (2018). In the centre of the domain a pulse of high fluid pressure is applied to a narrow band ($w_0 = 1$ cm), mimicking the initial crack that allows for fluid flow into the granulite host-rock. Introducing the shorthand notation $\Delta P_{\mathrm{r}} = P_{\mathrm{r}} - P_{\mathrm{bg}}$, with P_{r} the reaction pressure, that expresses the increase in pressure needed for the granulite to cross the reaction, it is clear that the pressure pulse must be greater than ΔP_{r} to trigger eclogitisation. The pressure of the fluid pulse is set at $\Delta P_f = 10$ kbar, consistent with estimates of possible overpressure in Holsnøy (Centrella, 2019; Jamtveit et al., 2018b; Moulas et al., 2022), and fluid pressure pulses in other geological contexts (e.g. Vrijmoed et al., 2009; Viete et al., 2018). A study of the effect of ΔP_f is presented in the result section. To assert the robustness of our approach, the initial pressure perturbation is applied as a step function: $P = 25$ kbar in the central crack and 15 kbar in the background.

2.4.2. Pressure pulse duration

Episodic high fluid pressure pulses in eclogite-facies rocks have been linked to dehydration reactions (Taetz et al., 2018; Hoover et al., 2022). Indeed, dehydration of adjacent units of the subducting plate can cause accumulation of pore fluids, resulting in periodic fluid pressure pulses that may cause brittle failure (Audet et al., 2009; Broadwell et al., 2019). Viete et al. (2018) showed that metamorphic rocks can record such fluid overpressures events.

The scenario we model is consistent with these observations. A fluid pressure pulse is applied in the central crack during a period $t_p = 50$ days, that can be interpreted as a single short pulse, or a series of very short-lived pressure pulses. This is consistent with the study of Malvoisin et al. (2020), who conclude that eclogitisation of dry granulite promotes further earthquake generation, which can self sustain the presence of high pressure pulses. It is also in agreement with the study of Putnis (2021) who argue that the transition in texture and composition from an untransformed granulite to an eclogite finger suggest a series of fluid pulses that advance the eclogitisation front into the granulite. Sporadic fluid pressure pulses can also be related to seismic aftershocks (Jamtveit et al., 2018a).

During the 50 days of the fluid pulse event, the model is an open system and the pressure in the initial crack is always $P_{\text{bg}} + \Delta P_f = 25$ kbar. This period is thereafter referred to as the open system period. After the first 50 days, the system closes and the pressure is free to drop in the initial crack. This period is referred to as the closed system period and lasts another 50 days, after which the simulation ends. Kaatz et al. (2021) likewise considered both open and closed systems, but in terms of amount of available fluid instead of fluid pressure.

2.4.3. Total solid mass

To assert the robustness of our approach, we set the background granulite porosity to 0 by using equation (9): given that $X_{\text{H}_2\text{O}} = 0$ in granulite, we set $\rho_T^s = \rho_s$ to ensure that $\phi = 0$. In other words, the solid mass per unit volume ρ_T^s must be equal to the density of granulite at 15 kbar, ie.e 2685 kg $\cdot$ m^{-3} (figure 2B). In the central crack, where the total pressure is higher than the reaction pressure, the granulite of density 2685 kg $\cdot$ m^{-3} is replaced by eclogite, with a density of 3228 kg $\cdot$ m^{-3}. As the total solid mass is conserved (equation 9), the porosity in the eclogite increases from 0 to 16% (figure 2C).

2.4.4. Permeability and fluid viscosity

In a Carman-Kozeny type relationship, the permeability is equal to $k_0\phi^3$, where k_0 is a permeability coefficient and ϕ the porosity. In our model, eclogite porosity is around 0.16 (figure 2C). Using a permeability coefficient $k_0 = 10^{-19}$ m^2 yields an eclogite permeability of 4×10^{-22} m^2, consistent with estimates of crustal permeability by Shmonov et al. (2003) or Mindaleva et al. (2020). Granulite permeability is 0 because its porosity is 0. We use a dynamic fluid viscosity $\eta_f = 10^{-3}$ Pa $\cdot$ s, consistent with Audétat and Keppler (2004); Hack and Thompson (2011).

2.5. Validation of the model: resolution test

Resolution tests in both space and time were performed and are presented in supplementary figures S1 and S2. The results of tests for spatial resolution (S1) show convergence with increasing resolution, indicating that the employed finite differences discretisation is appropriate for HC modelling. We use 400 numerical grid points for the discretisation in space. One simulation can be computed in a few minutes on a standard laptop. Changing the time resolution (Courant–Friedrichs–Lewy condition, CFL) does not affect the predicted eclogite width (S2A) and has very little effects on the modelled pressure (S2B).

3. Results

3.1. Introductory examples

Figure 4 illustrates the behaviour of the two end-member cases described previously: open system with a fluid pulse continuous in time, and closed system with an instantaneous fluid pulse only during

Table 1: Model variables, and parameters used in the reference model. The equation determining the value of the model unknowns are indicated.

Symbol	Meaning	Unit	Value
P	Pressure	Pa	Eq. 12
ϕ	Porosity	-	Eq. 9, 13
ρ_T	Total mass per unit volume	$\mathrm{kg \cdot m^{-3}}$	Eq. 1, 14
ρ_s	Solid density	$\mathrm{kg \cdot m^{-3}}$	Eq. 11a
ρ_f	Fluid density	$\mathrm{kg \cdot m^{-3}}$	Eq. 11b
$X_{\mathrm{H_2O}}$	H_2O mass fraction	-	Eq. 11c
X_s	$1 - X_{\mathrm{H_2O}}$	-	
v_f	Fluid velocity	$\mathrm{m \cdot s^{-1}}$	
β	Solid compressibility	$\mathrm{Pa^{-1}}$	
T	Temperature	$^\circ$ C	700
P_{bg}	Background pressure	kbar	15
ΔP_f	Pulse fluid pressure	kbar	10
P_{r}	Reaction pressure	kbar	19.4
ΔP_{r}	$P_{\mathrm{r}} - P_{\mathrm{bg}}$	kbar	4.4
w_0	Width of initial crack	m	0.01
t_p	Duration of fluid pulse	days	50
ρ_T^s	Total solid mass per unit volume	$\mathrm{kg \cdot m^{-3}}$	2685
k_0	Permeability coefficient	$\mathrm{m^2}$	10^{-19}
η_f	Fluid viscosity	$\mathrm{Pa \cdot s}$	10^{-3}
n	Porosity exponent	-	3

the first numerical time step. The separate study of these two cases is useful to understand the following HC models that include both behaviours.

3.1.1. Open system

Figure 4A shows the behaviour of an open system. The high pressure perturbation in the centre of the domain is maintained, mimicking a continuous fluid supply, or a succession of fluid pressure pulses very close in time. This results in a continuous influx of mass into the system, since $\rho_T = \rho_T(P)$ (figure 2B). The rest of the configuration is identical to that presented in figure 3, except that the pressure perturbation is applied at only one numerical grid point. The continuous high pressure perturbation creates a pressure gradient between the crack and the granulite, leading to a fast hydration due to high Darcy flow. The eclogitisation zone expands rapidly from the crack, and is around 30 cm wide after 100 days.

3.1.2. Closed system

Figure 4B shows the behaviour of a closed system. Here, there is no additional supply of fluid pressure after the initial pressure perturbation, so the total mass present in the system is conserved. In a few days, the pressure profile evolves from the initial pressure perturbation to a plateau at the reaction pressure P_r. Afterwards, this plateau widens, although much more slowly than in the open system case, and persists long after the initial pressure perturbation has decayed.

3.2. Reference model

The time evolution of our reference model is presented in figure 5, with a total simulation time of 100 days. The system is open during the first half of the simulation, with a behaviour similar to figure 4A, and is closed during the second half, with a behaviour similar to figure 4B. Granulite instantaneously transforms into eclogite when the pressure leaves the granulite stability field. Because of the densification reaction, the eclogitisation zone is characterised by a high reaction-induced porosity. The eclogitisation zone spreads rapidly during the open system phase, from its initial width of 1 cm to 23 cm in 50 days (figure 5C). During the closed system stage the eclogite width increases only slightly, from 23 to 26 cm. Most of the widening occurs while the system is open, i.e. when a fluid pressure perturbation is active. At the end of the simulation the system is composed of a central eclogite region with $P = 19.4$ kbar and $\phi = 0.16$, with a sharp transition to the granulite region with $P = 15$ kbar and $\phi = 0$.

3.3. Parametric study

Simulations with varying duration of the pulse (t_p) and varying magnitude of the fluid pressure pulse (ΔP_f) were performed in order to determine how they affect the width of the eclogitisation zone (figure 6). Each simulation lasts for twice the duration of the fluid pulse: if $t_p = 50$ days, the simulation stops after 100 days. This allows us to compare the width of the eclogitisation zones in the same closed-system conditions. Every other parameter is the same as in the reference model (table 1, results in figure 5). Figure 6A shows that t_p and ΔP_f both contribute to increasing the width of the eclogitisation zone. Since eclogitisation occurs when P reaches the reaction pressure P_r, any model with a pressure pulse lower than $\Delta P_\mathrm{r} = 4.4$ kbar yields an eclogite width of 0.

Using the data displayed in figure 6A, we derived a formula for the width of an eclogitisation zone w as a function of t_p, ΔP_f, the width of the initial crack w_0 and the pressure increase required to eclogitise the granulite ΔP_r:

$$w \approx \alpha \sqrt{t_p(\Delta P_f - \Delta P_\mathrm{r})} + w_0, \tag{15}$$

where α is a constant determined empirically (with unit $\mathrm{m} \cdot \mathrm{Pa}^{-0.5} \cdot \mathrm{s}^{-0.5}$), and with t_p in seconds, ΔP_f and ΔP_r in Pascals, w and w_0 in metres. For a simulation time that is twice the duration of the open system, $\alpha = 4.76 \times 10^{-9}$ $\mathrm{m} \cdot \mathrm{Pa}^{-0.5} \cdot \mathrm{s}^{-0.5}$. This formula predicts w with little deviations from the

expected value (fig 6B, $r^2 = 0.997$), and is shown with the dotted line on figure 6C. For a simulation that only lasts until the system closes, w is predicted by equation (15) with a constant $\alpha = 4.47 \times 10^{-9}$ $\mathrm{m \cdot Pa^{-0.5} \cdot s^{-0.5}}$, and is shown with the dashed line on figure 6C. For a given ΔP_f, the time evolution of a model follows closely the widths predicted by equation (15).

Equation (15) shows that w has a square root dependency to the duration of the pulse t_p and to the pulse pressure overstep, relative to the reaction pressure, $\Delta P_f - \Delta P_\mathrm{r}$. For our reference model, with parameters $t_p = 4.3 \times 10^6$ s (50 days), $\Delta P_f = 10^9$ Pa, $\Delta P_\mathrm{r} = 4.4 \times 10^8$ Pa, and $w_0 = 0.01$ m, equation (15) yields $w = 0.24$ m, very close to the modelled value (figure 5). With parameters $t_p = 1.58 \times 10^8$ s (5 years), $\Delta P_f = 5 \times 10^8$ Pa, $\Delta P_\mathrm{r} = 4.4 \times 10^8$ Pa, and $w_0 = 0.01$ m, equation (15) yields $w = 0.47$ m.

4. Discussion

4.1. General features of the HC model

4.1.1. Time evolution of the system

Our results show that a very sharp pressure/porosity reaction front can propagate into a rock that has zero porosity, and hence, zero permeability. When the system is open and is driven by a high pressure gradient, eclogite width increases as a function of $\sqrt{t}$, which is typical of a diffusion process (e.g. Turcotte and Schubert, 2002), although the model does not explicitly solve a diffusion equation. ΔP_f is as important as t_p in the widening of eclogitisation zones: the pressure gradient determines how fast fluid can flow into the dry granulite.

When the system closes, the impermeability of granulite causes the fluid flow to be extremely slow, preventing fluid pressure diffusion. As a result, the high pressure plateau persists long after the end of the short-lived fluid pressure pulse (figures 4b, 5a), preserving the eclogitisation zone without any sustained pressure perturbation.

In our reference model (figure 5), a 25 cm wide eclogitisation zone can form in 100 days. This result is in agreement with that of Beinlich et al. (2020), who show that a reaction front can advance as fast as 10 cm per year, and with that of Taetz et al. (2018), who show that the duration of fluid-rock interaction in an eclogite mélange is 1 to 4 months. Our time estimate is also close to that of the hydro-mechanical-chemical model of Malvoisin et al. (2020), who conclude that eclogitisation of granulite can occur on the order of weeks.

4.1.2. Contribution of compressibility and eclogitisation to front propagation

Two processes contribute to an increase in solid density, and thus an increase in porosity: compressibility (increase in density of a given phase with increasing pressure) and eclogitisation (replacement of low density minerals by high density minerals). We compared the importance of these two processes by switching them on and off in different simulations (figure 7). The results show that both effects

contribute to the widening of the hydration zone. Eclogitisation generates most of the porosity by a significant increase in solid density, creating a stronger fluid flow and therefore a faster hydration front. Compressibility creates only little porosity, and therefore limited hydration.

4.1.3. Simplifications of the 1D HC model

Permeability. We consider a homogeneous, isotropic-permeability rock, whereas metamorphic rocks can have anisotropic permeabilities that are 1 to 2 orders of magnitude higher along the metamorphic fabric than in the normal direction (e.g. Acosta and Violay, 2020). This anisotropy cannot be included in our 1D model, but a 2D model would allow to model preferential growth of eclogite fingers in the direction of the metamorphic fabric of the granulite (Putnis et al., 2021).

Deformation. The aim of the present paper is to show, with a simple hydro-chemical model, that a high pressure perturbation, here caused by a fluid pulse, can propagate and drive a reactive porous fluid flow into an impermeable rock. Coupling shear deformation with hydro-chemical processes is out of the scope of this study, and an extension of our work would include viscous deformation in order to simulate the growth of shear zones. During deformation, the weak shear zones could exhibit larger pressures than the strong, dry host-rock, if they have a suitable orientation relative to the background stress field (Moulas et al., 2014; Jamtveit et al., 2018b). Stress caused by shear deformation could self sustain the high pressure anomaly in the shear zone and promote hydration front propagation and shear zone widening.

4.2. Applications to Holsnøy case study

4.2.1. High pressure sustainability in eclogite

In Holsnøy, eclogitisation occurs in (1) eclogite shear zones, that undergo deformation during eclogitisation (e.g. Austrheim, 1987; Bras et al., 2021), and (2) eclogite fingers that undergo static eclogitisation without associated macroscopic deformation (e.g. Jamtveit et al., 2000; Zertani et al., 2019; Baïsset et al., 2023). In our model we attribute overpressure only to a short-lived fluid pressure pulse, but additional causes of overpressure may be at play, in both eclogite fingers and shear zones.

Eclogite fingers. Consistent with our work, Putnis (2021) inferred a pressure gradient from the host-rock granulite to an eclogite finger, deducing that the eclogite finger experienced a higher pressure. It was also shown (Jamtveit et al., 2000; Baïsset et al., 2023) that static eclogitisation of granulite causes perturbation in the local stress field, and could accelerate the propagation of fluids. Yamato et al. (2022) recently proposed that eclogitisation-induced densification of reacting granulite can generate sufficient shear stress to fail the rocks, and self-propagates eclogitisation in a finger-like structure. Reaction-induced densification therefore appears to be a likely mechanism that can sustain high pressures where eclogitisation takes place.

Shear zones. Sustained high pressure in eclogite shear zones can be achieved by weakening-induced overpressure (Jamtveit et al., 2018b), and numerous studies showed that eclogitisation me-

chanically weakens the granulite (Jolivet et al., 2005; Bras et al., 2021; Baïsset et al., 2023). This weakening can have crucial effects: Mancktelow (1993) showed that in deforming rocks, weak and strong layers can experience pressure differences of several kbar. Numerical simulations and analytical solutions show that the presence of a weak shear zone within a strong stressed lower crust can significantly increase the pressure inside the shear zone, potentially more than 10 kbar (Schmalholz and Podladchikov, 2013; Moulas et al., 2014; Jamtveit et al., 2018b; Moulas et al., 2022). The relevance of weakening induced pressure variations has also been suggested based on field observations (e.g. Luisier et al., 2019). Weakening-induced pressure increase in eclogite shear zones is therefore probably significant (Jamtveit et al., 2018b) and could self-sustain overpressure in the eclogite, efficiently promoting fluid flow and further eclogitisation of the dry lower crust.

4.2.2. Metastability

As stated in the introduction, there is currently a debate on the pressure state of granulite in Holsnøy: the juxtaposition of eclogite and granulite regions can be either interpreted as (1) metastability of granulite at eclogite-facies conditions at 21 kbar (Bhowany et al., 2018) or (2) local pressure variations between granulite and eclogite (see discussion in Putnis et al., 2021). Here, we show that the local pressure hypothesis is consistent with widening of eclogitisation zones. However, we can also test the metastable hypothesis with two modifications to our numerical code:

1. Set the background pressure to 21 kbar, and
2. Change the reaction pressure from the value predicted by thermodynamic modelling (19.4 kbar) to 21.01 kbar, just above the background pressure.

By doing so, granulite is stable up to 21 kbar, at eclogite pressure conditions. Any little increase in pressure caused by fluid flow triggers the transition from granulite to eclogite, satisfyingly reproducing the metastable behaviour where the reaction is triggered by a fluid influx. We here use a pressure of 21 kbar, close to the peak pressure estimated by Bhowany et al. (2018), but any pressure greater than P_r could be used. The general behaviour of the system is the same as in the stable scenario (see supplementary figure S3), the only difference being a wider eclogitisation zone in the metastable case (32 cm) compared to the stable case (24 cm). Although metastable granulite does not thermodynamically require a large pressure increase to transform into eclogite, a pressure gradient is still necessary to drive the fluid into the dry granulite by Darcy flow.

4.3. Reaction front propagation controlled by density of solid components

4.3.1. Theoretical considerations

We showed that widening of high pressure, hydrated zones is possible in the case of the granulite to eclogite reaction. In a general case, propagation of a hydration front in a dry rock is only possible if the metamorphic reaction induces porosity, otherwise the fluid could not flow and no hydration

would occur. In our hydro-chemical model without solid deformation, porosity is constrained by rock properties, which implies that changes in thermodynamic properties caused by a metamorphic reaction are enough to predict whether it generates porosity. Since we consider that solid mass is only stored in the solid phase and not in the fluid phase, equation (9) can be used to describe the transformation of a protolith (rock a) with solid density ρ_s^a, mass fraction of volatile components in the solid $X^a_{\mathrm{H_2O}}$ and no porosity, into a transformed rock b with ρ_s^b, $X^b_{\mathrm{H_2O}}$ and reaction-induced porosity ϕ_r:

$$\rho_T^s = \rho_s^a(1 - X^a_{\mathrm{H_2O}}) = \rho_s^b(1 - X^b_{\mathrm{H_2O}})(1 - \phi_r). \tag{16}$$

Introducing the notation for the mass fraction of solid components in the solid $X_s = 1 - X_{\mathrm{H_2O}}$, equation (16) is used to compute the porosity generated by the reaction from rock a to rock b:

$$\phi_r = 1 - \frac{\rho_s^a X_s^a}{\rho_s^b X_s^b}. \tag{17}$$

The reaction generates porosity when ϕ_r is greater than 0, which is true only if:

$$\rho_s^b X_s^b > \rho_s^a X_s^a, \tag{18}$$

i.e. if the metamorphic reaction increases $\rho_s X_s$. Equation (18) can be rearranged as:

$$\frac{X_s^b}{X_s^a} > \frac{1}{\rho_s^b/\rho_s^a}. \tag{19}$$

Figure 8 shows the porosity created by the metamorphic reaction that transforms rock a into rock b with increasing pressure, excluding any solid deformation. No porosity is created in the white field because reactions in this field decrease the amount of solid mass stored in the solid ($\rho_s^b X_s^b < \rho_s^a X_s^a$). As expected from equation (19), the boundary between the two regions follows an inverse relationship. On figure 8, reactions are displayed on a prograde path: rock a is stable at low pressure and rock b at high pressure. Only the prograde reactions in the top right field of the diagram can propagate into a rock with no porosity, through a positive pressure pulse. If reactions in the white field (e.g. periclase $\rightarrow$ brucite) were instead displayed on a retrograde path (brucite $\rightarrow$ periclase), they would appear in the colour field, meaning that these reverse reactions can propagate a low pressure perturbation into a no porosity, high pressure region. This is for instance the case in the study of Schmalholz et al. (2020), who show with numerical model similar to ours that a front of low pressure, dense periclase can propagates into a high pressure, low density brucite region.

Two situations are hence capable of generating a reaction/pressure front that propagates into a zero-porosity region. If the high pressure rock has a higher $\rho_s X_s$ than the low pressure rock (colour field in figure 8), a sharp high pressure, high density front can propagate into a low pressure, low-density rock. Conversely, if the high pressure rock has a lower $\rho_s X_s$ than the low pressure rock (white field), a sharp low pressure, high density front can propagate into a high pressure, low-density rock. Such situations were also discussed by Malvoisin et al. (2015), although they described these systems

in terms of negative and positive Clapeyron slopes instead of, respectively, increase and decrease of $\rho_s X_s$. They showed that a sharp pressure/porosity front propagates only for negative Clapeyron slope and positive pressure pulses, and for positive Clapeyron slopes and negative pressure pulses.

4.3.2. Applications

Even if X_s and ρ_s changes contribute in exactly the same manner to reaction-induced porosity, in natural metamorphic reaction changes in density are generally much greater than changes in X_s. For instance the data of Centrella (2019) shows that eclogitisation of granulite increases density by 7%, but decreases X_s by only 0.5%. Therefore, even if in a general case an increase in $\rho_s X_s$ is required, in most natural cases an increase in ρ_s (a decrease in solid volume) should be sufficient to explain reaction-induced porosity in a high pressure front.

Consistent with our work, Putnis and John (2010) showed that increased porosity enhances fluid transport, mineral replacement and propagation of a reaction front. Our results suggest that in purely rigid, non-deforming rocks, only reactions which decrease the solid volume (i.e. increase solid density) would be able to efficiently propagate through generation of porosity. Hövelmann et al. (2012) experimentally showed that carbonation reaction of peridotite fills the pre-existing porosity because the reaction increases the rock volume, which ultimately self-limits the reaction.

However there is evidence that other mechanisms can generate porosity at the reactive interface, even when the reaction lowers the solid density. Jamtveit et al. (2008) showed that stress induced by volume increase can generate extensive (micro-)fracturing, which creates a connected network that allows fluid transport. In a locality nearby Holsnøy, Moore et al. (2020) described sharp amphibolitisation fronts into granulite, with enhanced permeability/porosity in the less dense amphibolite. They showed evidence of abundant mass redistribution, which our model does not account for, resulting in an overall mass loss during fluid rock interaction. This can explain generation of porosity even though amphibolitisation increases the rock volume.

Shear zones in Monte Mucrone (Italian Alps) studied by Früh-Green (1994) do not show evidence of widening. Their chemical analysis shows that in the meta-diorite protolith and the eclogite shear zone, X_s and ρ_s are almost identical ($X_s^2/X_s^1 = 0.994$, $\rho_s^2/\rho_s^1 = 1.007$). This indicates that the reaction, close to [1, 1] coordinates on figure 8, generate neither porosity nor fracturing induced by volume increase, and thus no hydration front that propagates into the protolith.

In general, retrogression of high grade rocks replaces dense and anhydrous minerals (garnet, pyroxene) by low density and/or hydrous minerals (amphiboles, mica, chlorite, plagioclase). Low grade rocks therefore generally have a lower rock density and a higher water content, i.e. a lower ρ_X than higher grade rocks (e.g. Hacker et al., 2003). Our work implies that retrogression must be supported by some other porosity-generating mechanisms, such as mass transport or brittle deformation caused by volume increase. We suggest that in absence of such mechanisms, retrogression may be limited

and high grade rocks may be preserved during their exhumation.

4.4. Hydraulic diffusion

4.4.1. Hydraulic diffusion during eclogitisation

Kaatz et al. (2022) showed that H_2O content variations across eclogite shear zones are affected by solid state diffusion of hydrogen, but their work does not show if solid state diffusion plays a significant role in the widening of the eclogitisation zones. Putnis and John (2010) showed that mineral replacement during metamorphic reactions occur by fluid transport associated with reaction-induced porosity, rather than solid state diffusion. For this reason, our model includes Darcy flow instead of solid state fluid diffusion of hydrogen and oxygen atoms into the crystalline lattice, like some papers have done in the past to model eclogitisation (Bras et al., 2021).

Nevertheless, figure 6 shows that the front propagation distance is proportional to the square root of time, implying that fluid transport by reactive Darcy flow is a diffusive transport, termed hydraulic diffusion (e.g. Connolly, 1997). By analogy with a general diffusion law, a hydraulic diffusivity constant D_H can be used to relate the characteristic length of diffusion L and the characteristic time of diffusion τ:

$$L = \sqrt{D_H \tau}. \tag{20}$$

Using this relationship, a hydraulic diffusivity can be determined for the granulite-eclogite case when a fluid pulse is active, using our empirically derived equation (15) with $\alpha = 4.47 \times 10^{-9}$ m $\cdot$ Pa$^{-0.5}\cdot$s$^{-0.5}$. The characteristic length of diffusion is the distance travelled by the hydration front, in our case $L = \frac{w-w0}{2}$. The characteristic time is the duration of the fluid pressure pulse ($\tau = t_p$). Reformulating equation (15) with these parameters yields

$$L = \sqrt{\left(\frac{4.47 \times 10^{-9}}{2}\right)^2 (\Delta P_f - \Delta P_\mathrm{r})\tau}. \tag{21}$$

The ratio of permeability coefficient to fluid viscosity k_0/η_f has a first order control on the timing of the hydration process. Tests for varying simulation times t and k_0/η_f indeed show that the results of our model are not only a function of t, but rather $t \times k_0/\eta_f$ (supplementary figure S4). As an example, in a simulation where k_0/η_f is 10 times greater than our reference model, the results displayed on figure 5 appear after 10 days instead of 100. We can therefore introduce the k_0/η_f ratio in equation (21):

$$L = \sqrt{0.05 \frac{k_0}{\eta_f} (\Delta P_f - \Delta P_\mathrm{r})\tau}. \tag{22}$$

Substituting equation (22) into equation (20) yields an equation for D_H:

$$D_H \approx 0.05 \frac{k_0}{\eta_f} (\Delta P_f - \Delta P_\mathrm{r}). \tag{23}$$

In our reference model where $k_0/\eta_f = 10^{-16}$ m$^3\cdot$s $\cdot$ kg^{-1} and $\Delta P_f - \Delta P_\mathrm{r} = 5.6 \times 10^8$ Pa, equation 23 yields a hydraulic diffusivity in the order of 10^{-9} m$^2\cdot$s^{-1}. This is orders of magnitude higher than

solid state diffusivity of hydrogen or oxygen atoms in rock forming minerals, that range from 10^{-11} to 10^{-18} $m^2 \cdot s^{-1}$, in most cases 10^{-13} to 10^{-15} $m^2 \cdot s^{-1}$, at temperatures relevant for this study (Ingrin and Blanchard, 2006; Farver, 2010). Our work therefore shows that the propagation of a reacting hydration front by porous flow is a diffusive process that is potentially orders of magnitudes faster than solid-state diffusion.

4.4.2. General hydraulic diffusivity

Equation (23) applies to our granulite to eclogite model. In a general case, the width of the hydration zone must also be controlled by the reaction-induced porosity ϕ_r. Tests with varying ϕ_r (figure 9) reveal that the width of the hydration zone is proportional to ϕ_r, therefore:

$$L = \frac{\phi_r}{\phi_r^e} \sqrt{0.05 \frac{k}{\eta_f} (\Delta P_f - \Delta P_\mathrm{r}) \tau}, \tag{24}$$

where $\phi_r^e = 0.1625$ is the porosity induced by eclogitisation of granulite (figure 2C). Additionally, since ϕ_r is thermodynamically constrained by equation (17), we can substitute ϕ_r for properties of the protolith (ρ_s^a, X_s^a) and of the transformed rock (ρ_s^b, X_s^b):

$$L = \left(1 - \frac{\rho_s^a X_s^a}{\rho_s^b X_s^b}\right) \sqrt{1.9 \frac{k}{\eta_f} (\Delta P_f - \Delta P_\mathrm{r}) \tau}. \tag{25}$$

Substituting equation (25) into equation (20) yields a general equation for the hydraulic diffusivity D_H that can be estimated for any reaction:

$$D_H = 1.9 \left(1 - \frac{\rho_s^a X_s^a}{\rho_s^b X_s^b}\right)^2 \frac{k}{\eta_f} (\Delta P_f - \Delta P_\mathrm{r}). \tag{26}$$

5. Conclusion

We present a physically consistent hydro-chemical model of eclogitisation of impermeable granulite, that can explain the widening of eclogite shear zones and eclogite fingers in Holsnøy. Our work shows that hydration of a zero-porosity rock is possible only if density changes controlled by pressure changes are taken into account: solid compressibility or metamorphic reactions. Fluid overpressure will drive a reactive, porous fluid flow into an impermeable rock, as long as the high-pressure rock is denser than its impermeable protolith. Our model can simulate any reaction inducing density changes, as well as metastable scenarios.

In our model without mechanics, overpressure is only caused by a fluid pressure pulse, and future work should take solid deformation into account. Deformation could enhance the overpressure and subsequent reactive fluid flow, as long as the high pressure rock is mechanically weaker than its protolith.

Local pressure perturbations of several kbars, caused by fluid pulses or weakening-induced overpressure, can induce reaction front propagation at a rate of tens of centimetres per year, as long as

the pressure perturbation is present. The rate at which the reaction front propagates is typical of a diffusive process. This complex and coupled hydro-chemical process can hence be approximated by a diffusion law, where the diffusivity can be calculated for any reaction from the pressure gradients and rock properties.

6. Acknowledgments

We thank Marie Baïsset for her help in the field and for providing photograph 1B, and Loïc Labrousse for multiple discussions about eclogitisation processes. This work has been partially financially supported by the INSU SYSTER program (AO Tellus), and by the University of Lausanne. P.Y. thanks the Institut Universitaire de France for financial support. We thank 2 anonymous reviewers for their very insightful comments that have improved and clarified the paper, and Alex Webb for editorial handling.

7. Data Availability

All numerical results have been generated with a self-developed MATLAB code, which is available on the platform Zenodo under: https://doi.org/10.5281/zenodo.7966767.

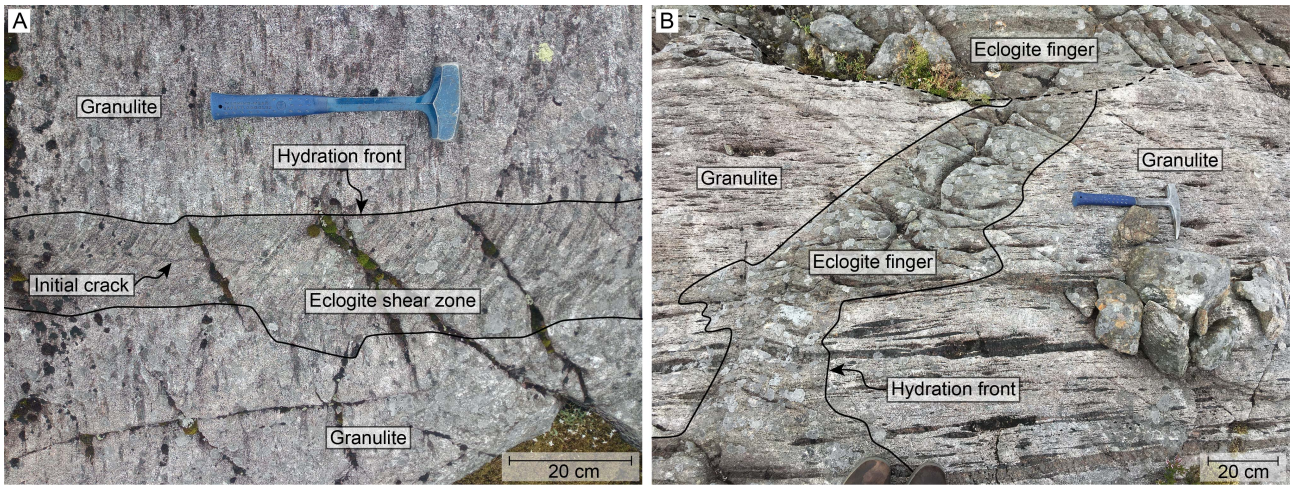

Figure 1: Photographs from Holsnøy (western Norway), showing a halo of eclogitisation overprinting the granulite. (A) Eclogite shear zone (eclogitisation associated with deformation); 60°35'11"N, 5°07' 34"E. The shear zone develops around a narrow central crack. (B) Eclogite finger (no deformation); 60°35'27"N, 5°00'44"E.

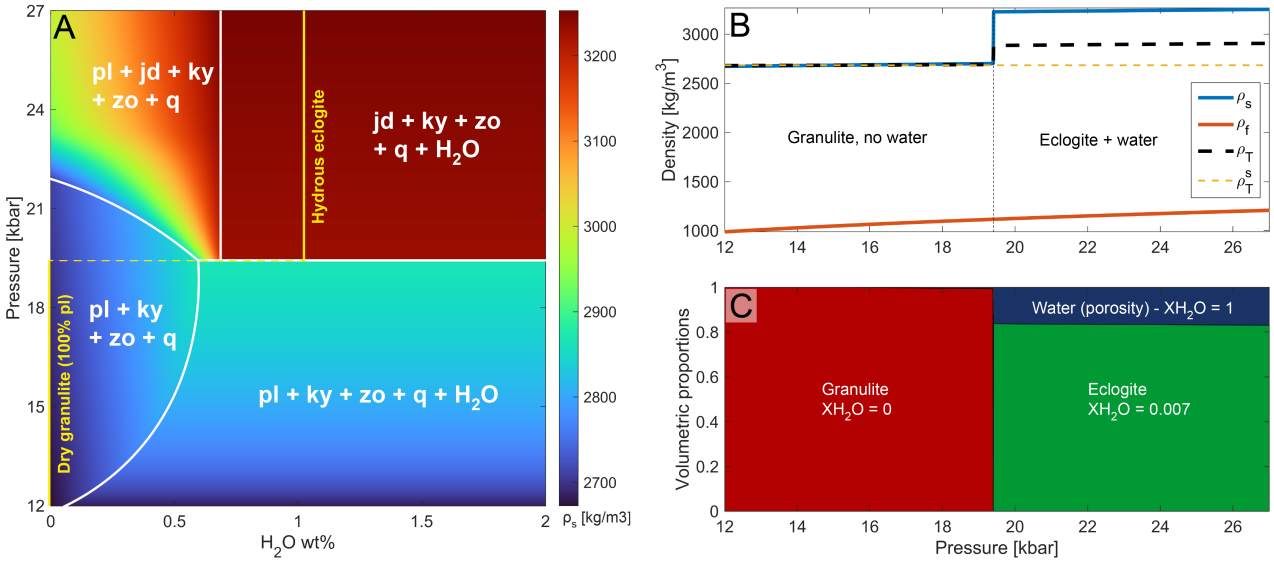

Figure 2: Thermodynamic data used in the model. (A) Perple_X pseudosection used to mimic the stable mineralogical assemblages resulting from destabilisation of anorthosite, as a function of water content and pressure. The yellow line shows the H_2O wt% conditions at which we retrieve solid density data: dry conditions for granulite at low pressure, and 1 wt% (saturated in H_2O) for eclogite at high pressure. Abbreviations after Holland and Powell (1998): pl: plagioclase, ky: kyanite, zo: zoisite, q: quartz, jd: jadeite. (B) Corresponding 1D look-up tables for solid (ρ_s) and fluid (ρ_f) density as a function of pressure, and total density (ρ_T) look-up table calculated from equation (12). The total solid mass (ρ_T^s) is a constant value of 2685 kg $\cdot$ m^{-3}. (C) Phase composition of the system. At 15 kbar, granulite has zero porosity.

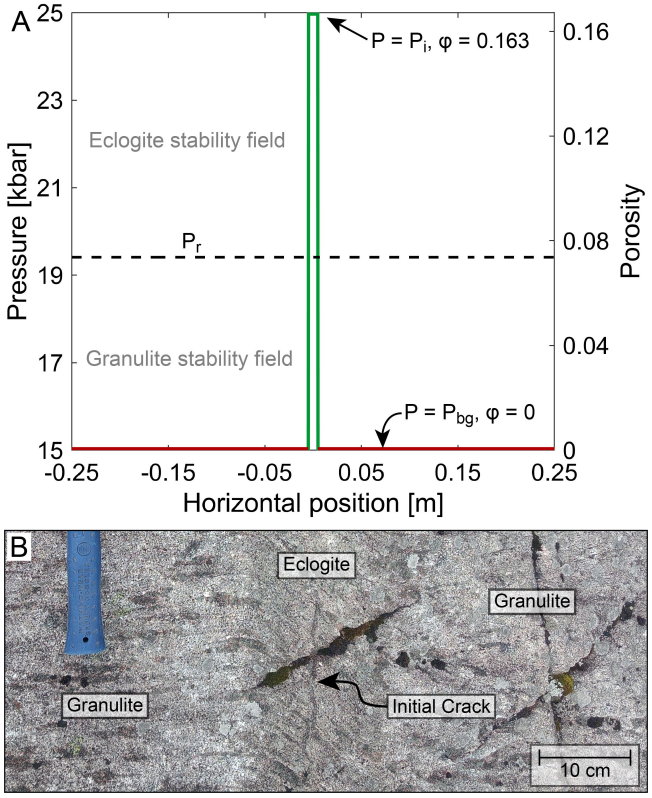

Figure 3: Model configuration. (A) Initial profiles of pressure and porosity. All the domain is made up of granulite with no porosity initially placed at 15 kbar (P_{bg}, red line), except the central narrow crack that is submitted to a high fluid pressure pulse. This initial pressure P_{i}, higher than the reaction pressure P_{r} (dotted line), is enough to trigger eclogitisation and generate porosity (green line). (B) Detail of the shear zone from photograph 1A (top view) with features comparable our configuration: a central narrow crack cutting through the granulite, from which the eclogitisation front propagates.

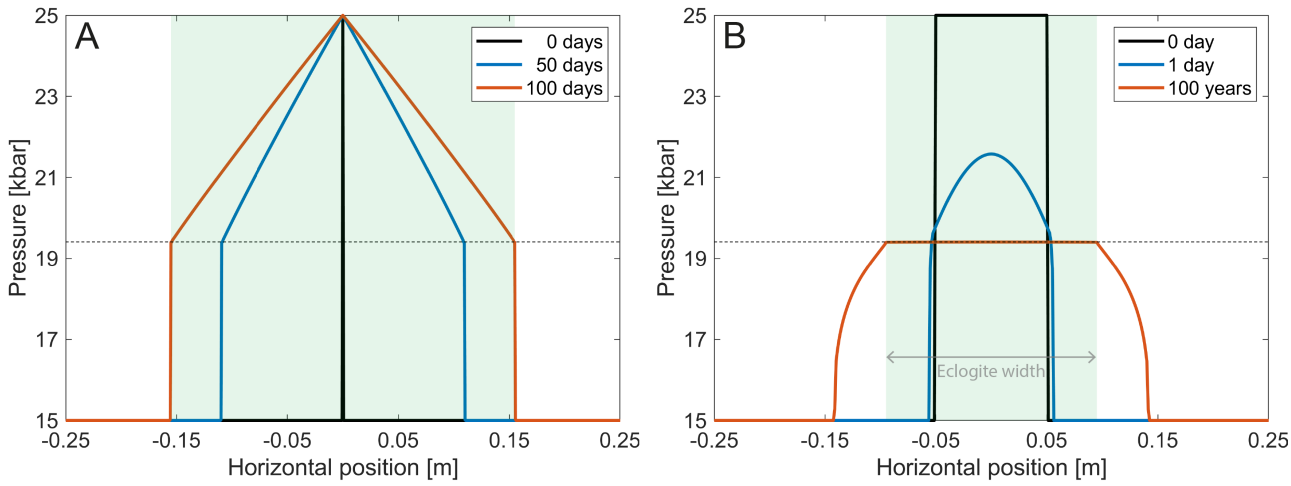

Figure 4: Introductory examples to the hydro-chemical model. Light green areas represent the eclogite width after 100 years. A: Open system. In the centre of the domain, the pressure is always fixed at 25 kbar as a boundary condition. This corresponds to a fluid pulse that is continuously supplied by the central crack. B: Closed system. There is no fluid supply except the initial step-like pressure profile that decays rapidly, and then slowly diffuses into the granulite. Notice the difference in time scales between A and B.

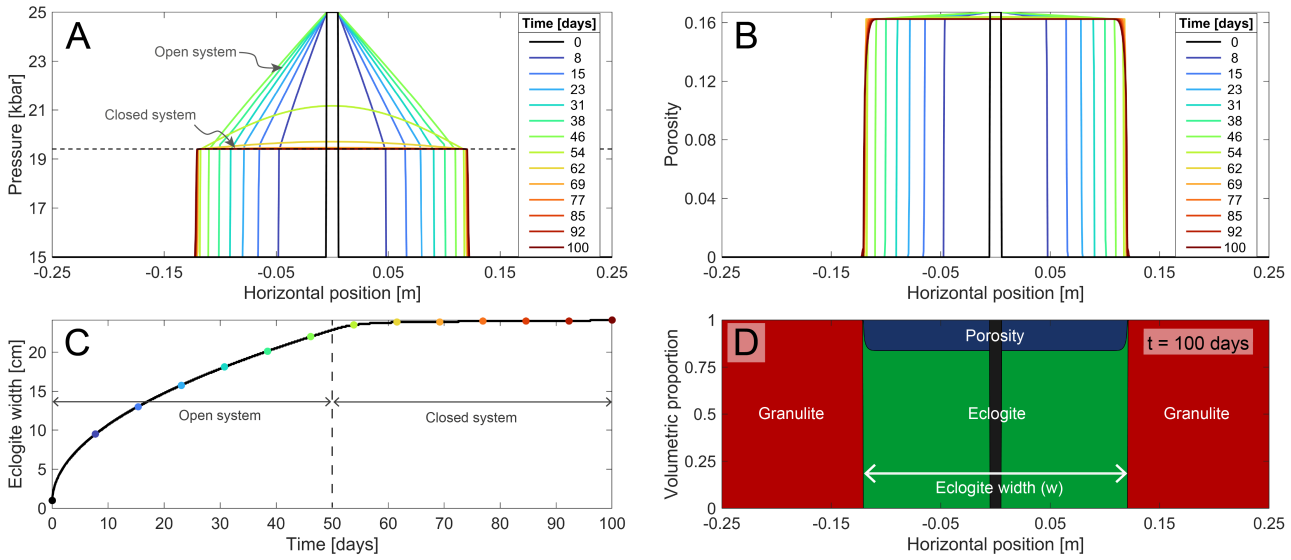

Figure 5: Result of a simulation after 100 days. The fluid pulse lasts 50 days with a behaviour similar to the model of figure 4A, and then the fluid supply ends, rapidly shifting to the behaviour shown in figure 4B. (A) Evolution of the pressure and (B) evolution of the porosity with time. (C) Evolution of the width of the eclogitisation zone over time. The colour dots correspond to profiles in A and B. (D) Phase composition at the end of the simulation (100 days). The narrow black region shows the region where the fluid pulse is applied, of width $w_0 = 1$ cm. It is already eclogitised at the start of the simulation.

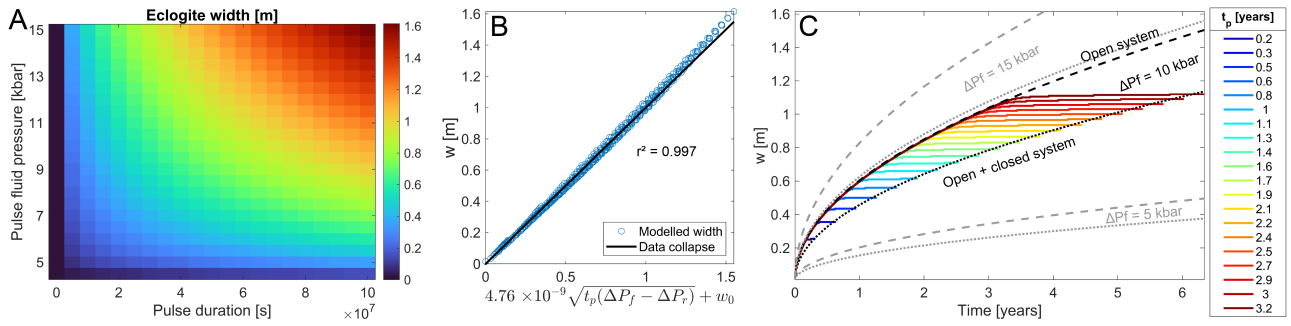

Figure 6: Parametric study. (A) Eclogitisation zone width w as a function of the duration of the fluid pulse t_p and of the fluid pressure of the pulse ΔP_f. The duration of the simulation is $2 \times t_p$ for all simulations. (B) Data collapse for the eclogite width at the end of the simulation (open + closed system). See text for details and explanation of the parameters. (C) Time evolution of the eclogite width w for different t_p and ΔP_f. The colour lines show the modelled time evolution for different t_p and $\Delta P_f = 10$ kbar. The dotted lines show the eclogite width time evolution predicted in 6B and equation (15) with $\alpha = 4.76 \times 10^{-9}$, for the indicated ΔP_f. The dashed lines show the eclogite width time evolution at the end of the open system predicted by equation (15) with $\alpha = 4.47 \times 10^{-9}$. The predictive lines aligns closely to the modelled colour lines. Colour lines for the other ΔP_f are not plotted to reduce cluttering on the diagram, but they would align with the dotted and dashed lines in a similar fashion.

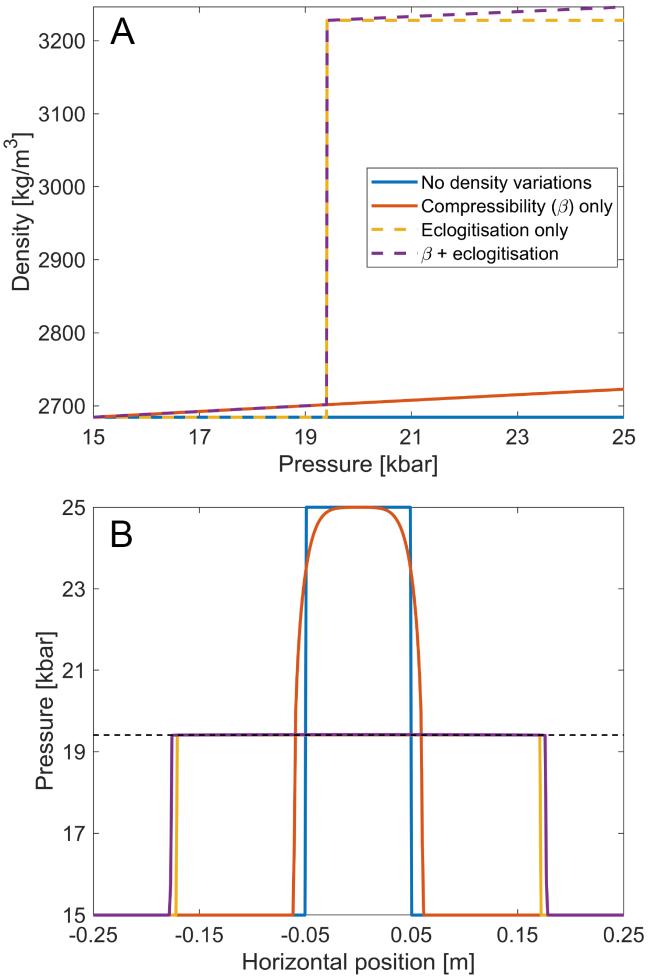

Figure 7: Effect of density changes on the widening of an eclogitisation zone. (A) Solid density as a function of pressure for 4 different scenarios. Blue: the solid is incompressible and non-reactive; its density never increases. Orange: the solid is non-reactive; its density only increases due to compressibility. Yellow: the solid is incompressible, its density only increases due to transformation of granulite into eclogite. Purple: the solid density increases due to compressibility and transformation of granulite into eclogite, as used throughout this study. (B) Pressure profiles after 100 days. The blue profile is identical to the initial pressure profile. Thickness of the initial perturbation (compared to figures 3, 5) was increased for clearer visualisation.

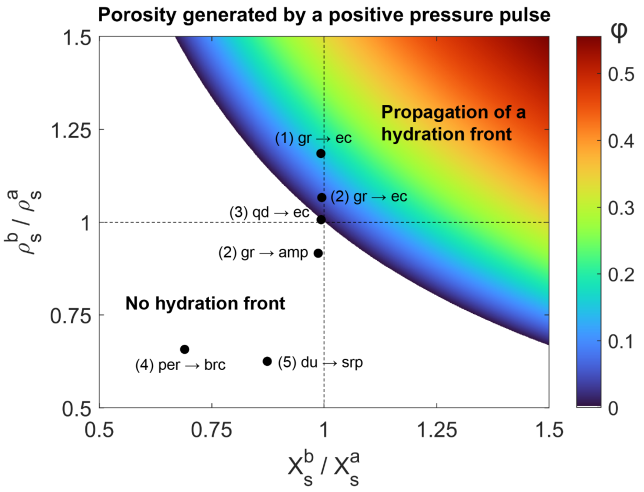

Figure 8: Porosity generated by the transformation of a low pressure rock a (with solid density ρ_s^a and proportion of non volatile component X_s^a) into a high pressure rock b (with ρ_s^b and X_s^b). Porosity is created only when the reaction increases the solid mass stored in the solid, i.e. $X_s^b \rho_s^b > X_s^a \rho_s^a$. Reactions in the white field do not generate porosity. Abbreviations: gr = granulite; ec = eclogite; amp = amphibolite; qd = quartz-diorite; per = periclase; brc = brucite; du = dunite; srp = serpentinite; atg = antigorite. Source of ρ_s and X_s data: (1) This work, (2) Centrella (2019); (3) Früh-Green (1994); (4) Schmalholz et al. (2020); (5) Malvoisin et al. (2021).

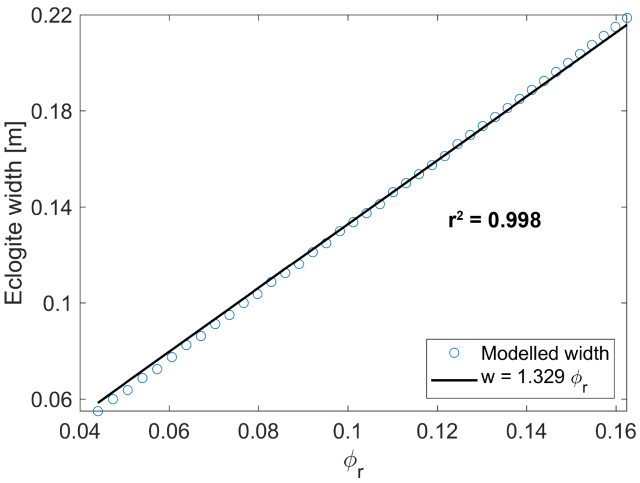

Figure 9: Linear fit of hydration zone width as a function of reaction-induced porosity ϕ_r. The width of the hydration zone increases linearly with ϕ_r. The parameters of the simulations are the same as in the reference model, except $w_0 = 0$ m. The simulation ends when the system closes, after 50 days. ϕ_r is set by modifying the densities of granulite and eclogite in the look-up table.

References

Acosta, M., Violay, M., 2020. Mechanical and hydraulic transport properties of transverse-isotropic gneiss deformed under deep reservoir stress and pressure conditions. International journal of rock mechanics and mining sciences 130, 104235. doi:https://doi.org/10.1016/j.ijrmms.2020.104235.

Andersen, T.B., Jamtveit, B., Dewey, J.F., Swensson, E., 1991. Subduction and eduction of continental crust: Major mechanisms during continent-continent collision and orogenic extensional collapse, a model based on the south norwegian caledonides. Terra Nova 3, 303–310. doi:https://doi.org/10.1111/j.1365-3121.1991.tb00148.x.

Arbogast, T., Hesse, M.A., Taicher, A.L., 2017. Mixed methods for two-phase darcy–stokes mixtures of partially melted materials with regions of zero porosity. SIAM Journal on Scientific Computing 39, B375–B402. doi:https://doi.org/10.1137/16M1091095.

Audet, P., Bostock, M.G., Christensen, N.I., Peacock, S.M., 2009. Seismic evidence for overpressured subducted oceanic crust and megathrust fault sealing. Nature 457, 76–78. doi:https://doi.org/10.1038/nature07650.

Audétat, A., Keppler, H., 2004. Viscosity of fluids in subduction zones. Science 303, 513–516. doi:https://doi.org/10.1126/science.1092282.

Austrheim, H., 1987. Eclogitization of lower crustal granulites by fluid migration through shear zones. Earth and Planetary Science Letters 81, 221–232. doi:https://doi.org/10.1016/0012-821X(87)90158-0.

Austrheim, H., 1998. Influence of fluid and deformation on metamorphism of the deep crust and consequences for the geodynamics of collision zones, in: Hacker, B.R., Liou, J.G. (Eds.), When Continents Collide: Geodynamics and Geochemistry of Ultrahigh-Pressure Rocks. Springer Netherlands, Dordrecht, pp. 297–323. doi:https://doi.org/10.1007/978-94-015-9050-1_12.

Austrheim, H., 2013. Fluid and deformation induced metamorphic processes around moho beneath continent collision zones: Examples from the exposed root zone of the caledonian mountain belt, w-norway. Tectonophysics 609, 620–635. doi:https://doi.org/10.1016/j.tecto.2013.08.030.

Baïsset, M., Labrousse, L., Yamato, P., Schubnel, A., 2023. Twinning and partial melting as early weakening processes in plagioclase at high pressure: insights from holsnøy (scandinavian caledonides, norway). Contributions to Mineralogy and Petrology 178, 19. doi:https://doi.org/10.1007/s00410-023-01998-x.

Beinlich, A., John, T., Vrijmoed, J.C., Tominaga, M., Magna, T., Podladchikov, Y.Y., 2020. Instantaneous rock transformations in the deep crust driven by reactive fluid flow. Nature Geoscience 13, 307–311. doi:https://doi.org/10.1038/s41561-020-0554-9.

Bhowany, K., Hand, M., Clark, C., Kelsey, D.E., Reddy, S.M., Pearce, M.A., Tucker, N.M., Morrissey, L.J., 2018. Phase equilibria modelling constraints on p–t conditions during fluid catalysed conversion of granulite to eclogite in the bergen arcs, norway. Journal of Metamorphic Geology 36, 315–342. doi:https://doi.org/10.1111/jmg.12294.

Bingen, B., Davis, W.J., Austrheim, H., 2001. Zircon u-pb geochronology in the bergen arc eclogites and their proterozoic protoliths, and implications for the pre-scandian evolution of the caledonides in western norway. Geological Society of America Bulletin 113, 640–649. doi:https://doi.org/10.1130/0016-7606(2001)113<0640:ZUPGIT>2.0.CO;2.

Bras, E., Baïsset, M., Yamato, P., Labrousse, L., 2021. Transient weakening during the granulite to eclogite transformation within hydrous shear zones (holsnøy, norway). Tectonophysics 819, 229026. doi:https://doi.org/10.1016/j.tecto.2021.229026.

Broadwell, K.S., Locatelli, M., Verlaguet, A., Agard, P., Caddick, M.J., 2019. Transient and periodic brittle deformation of eclogites during intermediate-depth subduction. Earth and Planetary Science Letters 521, 91–102. doi:https://doi.org/10.1016/j.epsl.2019.06.008.

Centrella, S., 2019. The granulite-to eclogite-and amphibolite-facies transition: a volume and mass transfer study in the lindås nappe, bergen arcs, west norway. Geological Society, London, Special Publications 478, 241–264. doi:https://doi.org/10.1144/SP478.9.

Connolly, J., 1997. Devolatilization-generated fluid pressure and deformation-propagated fluid flow during prograde regional metamorphism. Journal of Geophysical Research: Solid Earth 102, 18149–18173. doi:https://doi.org/10.1029/97JB00731.

Connolly, J.A., 2005. Computation of phase equilibria by linear programming: a tool for geodynamic modeling and its application to subduction zone decarbonation. Earth and Planetary Science Letters 236, 524–541. doi:https://doi.org/10.1016/j.epsl.2005.04.033.

Costa, A., 2006. Permeability-porosity relationship: A reexamination of the kozeny-carman equation based on a fractal pore-space geometry assumption. Geophysical research letters 33. doi:https://doi.org/10.1029/2005GL025134.

Dahlen, F., 1992. Metamorphism of nonhydrostatically stressed rocks. American Journal of Science 292, 184–198. doi:https://doi.org/10.2475/ajs.292.3.184.

Farver, J.R., 2010. Oxygen and hydrogen diffusion in minerals. Reviews in Mineralogy and Geochemistry 72, 447–507. doi:https://doi.org/10.2138/rmg.2010.72.10.

Früh-Green, G.L., 1994. Interdependence of deformation, fluid infiltration and reaction progress recorded in eclogitic metagranitoids (sesia zone, western alps). Journal of Metamorphic Geology 12, 327–343. doi:https://doi.org/10.1111/j.1525-1314.1994.tb00026.x.

Gerya, T., 2019. Introduction to numerical geodynamic modelling. Cambridge University Press. doi:https://doi.org/10.1017/9781316534243.

Hack, A.C., Thompson, A.B., 2011. Density and viscosity of hydrous magmas and related fluids and their role in subduction zone processes. Journal of Petrology 52, 1333–1362. doi:https://doi.org/10.1093/petrology/egq048.

Hacker, B.R., Abers, G.A., Peacock, S.M., 2003. Subduction factory 1. theoretical mineralogy, densities, seismic wave speeds, and h2o contents. Journal of Geophysical Research: Solid Earth 108. doi:https://doi.org/10.1029/2001JB001127.

Hetényi, G., Cattin, R., Brunet, F., Bollinger, L., Vergne, J., Nábělek, J.L., Diament, M., 2007. Density distribution of the india plate beneath the tibetan plateau: Geophysical and petrological constraints on the kinetics of lower-crustal eclogitization. Earth and Planetary Science Letters 264, 226–244. doi:https://doi.org/10.1016/j.epsl.2007.09.036.

Holland, T., Powell, R., 1998. An internally consistent thermodynamic data set for phases of petrological interest. Journal of metamorphic Geology 16, 309–343. doi:https://doi.org/10.1111/j.1525-1314.1998.00140.x.

Hoover, W.F., Penniston-Dorland, S., Baumgartner, L., Bouvier, A.S., Dragovic, B., Locatelli, M., Angiboust, S., Agard, P., 2022. Episodic fluid flow in an eclogite-facies shear zone: Insights from li isotope zoning in garnet. Geology 50, 746–750. doi:https://doi.org/10.1130/G49737.1.

Hövelmann, J., Austrheim, H., Jamtveit, B., 2012. Microstructure and porosity evolution during experimental carbonation of a natural peridotite. Chemical Geology 334, 254–265. doi:https://doi.org/10.1016/j.chemgeo.2012.10.025.

Incel, S., Hilairet, N., Labrousse, L., John, T., Deldicque, D., Ferrand, T., Wang, Y., Renner, J., Morales, L., Schubnel, A., 2017. Laboratory earthquakes triggered during eclogitization of lawsonite-bearing blueschist. Earth and Planetary Science Letters 459, 320–331. doi:https://doi.org/10.1016/j.epsl.2016.11.047.

Ingrin, J., Blanchard, M., 2006. Diffusion of hydrogen in minerals. Reviews in Mineralogy and Geochemistry 62, 291–320. doi:https://doi.org/10.2138/rmg.2006.62.13.

Jackson, J.A., Austrheim, H., McKenzie, D., Priestley, K., 2004. Metastability, mechanical strength, and the support of mountain belts. Geology 32, 625–628. doi:https://doi.org/10.1130/G20397.1.

Jamtveit, B., Austrheim, H., Malthe-Sørenssen, A., 2000. Accelerated hydration of the earth's deep crust induced by stress perturbations. Nature 408, 75–78. doi:https://doi.org/10.1038/35040537.

Jamtveit, B., Ben-Zion, Y., Renard, F., Austrheim, H., 2018a. Earthquake-induced transformation of the lower crust. Nature 556, 487–491. doi:https://doi.org/10.1038/s41586-018-0045-y.

Jamtveit, B., Malthe-Sørenssen, A., Kostenko, O., 2008. Reaction enhanced permeability during retrogressive metamorphism. Earth and Planetary Science Letters 267, 620–627. doi:https://doi.org/10.1016/j.epsl.2007.12.016.

Jamtveit, B., Moulas, E., Andersen, T.B., Austrheim, H., Corfu, F., Petley-Ragan, A., Schmalholz, S.M., 2018b. High pressure metamorphism caused by fluid induced weakening of deep continental crust. Scientific Reports 8, 17011. doi:https://doi.org/10.1038/s41598-018-35200-1.

Jamtveit, B., Petley-Ragan, A., Incel, S., Dunkel, K.G., Aupart, C., Austrheim, H., Corfu, F., Menegon, L., Renard, F., 2019. The effects of earthquakes and fluids on the metamorphism of the lower continental crust. Journal of Geophysical Research: Solid Earth 124, 7725–7755. doi:https://doi.org/10.1029/2018JB016461.

John, T., Schenk, V., 2006. Interrelations between intermediate-depth earthquakes and fluid flow within subducting oceanic plates: Constraints from eclogite facies pseudotachylytes. Geology 34, 557–560. doi:https://doi.org/10.1130/G22411.1.

Jolivet, L., Raimbourg, H., Labrousse, L., Avigad, D., Leroy, Y., Austrheim, H., Andersen, T.B., 2005. Softening trigerred by eclogitization, the first step toward exhumation during continental subduction. Earth and Planetary Science Letters 237, 532–547. doi:https://doi.org/10.1016/j.epsl.2005.06.047.

Kaatz, L., Reynes, J., Hermann, J., John, T., 2022. How fluid infiltrates dry crustal rocks during progressive eclogitization and shear zone formation: insights from h2o contents in nominally anhydrous minerals. Contributions to Mineralogy and Petrology 177, 72. doi:https://doi.org/10.1007/s00410-022-01938-1.

Kaatz, L., Zertani, S., Moulas, E., John, T., Labrousse, L., Schmalholz, S.M., Andersen, T.B., 2021. Widening of hydrous shear zones during incipient eclogitization of metastable dry and rigid lower crust—holsnøy, western norway. Tectonics 40, e2020TC006572. doi:https://doi.org/10.1029/2020TC006572.

Katz, R., Knepley, M.G., Smith, B., Spiegelman, M., Coon, E.T., 2007. Numerical simulation of geodynamic processes with the portable extensible toolkit for scientific computation. Physics of the Earth and Planetary Interiors 163, 52–68. doi:https://doi.org/10.1016/j.pepi.2007.04.016.

Labrousse, L., Hetényi, G., Raimbourg, H., Jolivet, L., Andersen, T.B., 2010. Initiation of crustal-scale thrusts triggered by metamorphic reactions at depth: Insights from a comparison between the himalayas and scandinavian caledonides. Tectonics 29, TC5002. doi:https://doi.org/10.1029/2009TC002602.

Landau, L.D., Lifshitz, E.M., 1980. Statistical Physics, Part 1, Course of Theoretical Physics. volume 5. Pergamon press, Oxford.

Llana-Fúnez, S., Wheeler, J., Faulkner, D.R., 2012. Metamorphic reaction rate controlled by fluid pressure not confining pressure: implications of dehydration experiments with gypsum. Contributions to Mineralogy and Petrology 164, 69–79. doi:https://doi.org/10.1007/s00410-012-0726-8.

Luisier, C., Baumgartner, L., Schmalholz, S.M., Siron, G., Vennemann, T., 2019. Metamorphic pressure variation in a coherent alpine nappe challenges lithostatic pressure paradigm. Nature communications 10, 4734. doi:https://doi.org/10.1038/s41467-019-12727-z.

Malvoisin, B., Austrheim, H., Hetényi, G., Reynes, J., Hermann, J., Baumgartner, L.P., Podladchikov, Y.Y., 2020. Sustainable densification of the deep crust. Geology 48, 673–677. doi:https://doi.org/10.1130/G47201.1.

Malvoisin, B., Podladchikov, Y.Y., Myasnikov, A.V., 2021. Achieving complete reaction while the solid volume increases: A numerical model applied to serpentinisation. Earth and Planetary Science Letters 563, 116859. doi:https://doi.org/10.1016/j.epsl.2021.116859.

Malvoisin, B., Podladchikov, Y.Y., Vrijmoed, J.C., 2015. Coupling changes in densities and porosity to fluid pressure variations in reactive porous fluid flow: Local thermodynamic equilibrium. Geochemistry, Geophysics, Geosystems 16, 4362–4387. doi:https://doi.org/10.1002/2015GC006019.

Mancktelow, N.S., 1993. Tectonic overpressure in competent mafic layers and the development of isolated eclogites. Journal of metamorphic Geology 11, 801–812. doi:https://doi.org/10.1111/j.1525-1314.1993.tb00190.x.

Menegon, L., Campbell, L., Mancktelow, N., Camacho, A., Wex, S., Papa, S., Toffol, G., Pennacchioni, G., 2021. The earthquake cycle in the dry lower continental crust: insights from two deeply exhumed terranes (musgrave ranges, australia and lofoten, norway). Philosophical transactions of the Royal Society A 379, 20190416. doi:https://doi.org/10.1098/rsta.2019.0416.

Miller, S.A., 2013. The role of fluids in tectonic and earthquake processes. Advances in geophysics 54, 1–46. doi:https://doi.org/10.1016/B978-0-12-380940-7.00001-9.

Mindaleva, D., Uno, M., Higashino, F., Nagaya, T., Okamoto, A., Tsuchiya, N., 2020. Rapid fluid infiltration and permeability enhancement during middle–lower crustal fracturing: Evidence from amphibolite–granulite-facies fluid–rock reaction zones, sør rondane mountains, east antarctica. Lithos 372, 105521. doi:https://doi.org/10.1016/j.lithos.2020.105521.

Moore, J., Beinlich, A., Piazolo, S., Austrheim, H., Putnis, A., 2020. Metamorphic differentiation via enhanced dissolution along high permeability zones. Journal of Petrology 61, egaa096. doi:https://doi.org/10.1093/petrology/egaa096.

Moulas, E., Burg, J.P., Podladchikov, Y., 2014. Stress field associated with elliptical inclusions in a deforming matrix: Mathematical model and implications for tectonic overpressure in the lithosphere. Tectonophysics 631, 37–49. doi:https://doi.org/10.1016/j.tecto.2014.05.004.

Moulas, E., Kaus, B., Jamtveit, B., 2022. Dynamic pressure variations in the lower crust caused by localized fluid-induced weakening. Communications Earth & Environment 3, 157. doi:https://doi.org/10.1038/s43247-022-00478-7.

Newton, R., Charlu, T., Kleppa, O., 1980. Thermochemistry of the high structural state plagioclases. Geochimica et Cosmochimica Acta 44, 933–941. doi:https://doi.org/10.1016/0016-7037(80)90283-5.

Plümper, O., John, T., Podladchikov, Y.Y., Vrijmoed, J.C., Scambelluri, M., 2017. Fluid escape from subduction zones controlled by channel-forming reactive porosity. Nature Geoscience 10, 150–156. doi:https://doi.org/10.1038/ngeo2865.

Putnis, A., 2021. Fluid–mineral interactions: controlling coupled mechanisms of reaction, mass transfer and deformation. Journal of Petrology 62, egab092. doi:https://doi.org/10.1093/petrology/egab092.

Putnis, A., Jamtveit, B., Austrheim, H., 2017. Metamorphic processes and seismicity: the bergen arcs as a natural laboratory. Journal of Petrology 58, 1871–1898. doi:https://doi.org/10.1093/petrology/egx076.

Putnis, A., John, T., 2010. Replacement processes in the earth's crust. Elements 6, 159–164. doi:https://doi.org/10.2113/gselements.6.3.159.

Putnis, A., Moore, J., Prent, A.M., Beinlich, A., Austrheim, H., 2021. Preservation of granulite in a partially eclogitized terrane: Metastable phenomena or local pressure variations? Lithos 400, 106413. doi:https://doi.org/10.1016/j.lithos.2021.106413.

Räss, L., Duretz, T., Podladchikov, Y., 2019. Resolving hydromechanical coupling in two and three dimensions: spontaneous channelling of porous fluids owing to decompaction weakening. Geophysical Journal International 218, 1591–1616. doi:https://doi.org/10.1093/gji/ggz239.

Räss, L., Utkin, I., Duretz, T., Omlin, S., Podladchikov, Y.Y., 2022. Assessing the robustness and scalability of the accelerated pseudo-transient method. Geoscientific Model Development 15, 5757–5786. doi:https://doi.org/10.5194/gmd-15-5757-2022.

Schmalholz, S.M., Moulas, E., Plümper, O., Myasnikov, A.V., Podladchikov, Y.Y., 2020. 2d hydro-mechanical-chemical modeling of (de)hydration reactions in deforming heterogeneous rock: The periclase-brucite model reaction. Geochemistry, Geophysics, Geosystems 21, e2020GC009351. doi:https://doi.org/10.1029/2020GC009351.

Schmalholz, S.M., Podladchikov, Y.Y., 2013. Tectonic overpressure in weak crustal-scale shear zones and implications for the exhumation of high-pressure rocks. Geophysical Research Letters 40, 1984–1988. doi:https://doi.org/10.1002/grl.50417.

Scott, D.R., Stevenson, D.J., 1986. Magma ascent by porous flow. Journal of Geophysical Research: Solid Earth 91, 9283–9296. doi:https://doi.org/10.1029/JB091iB09p09283.

Shi, F., Wang, Y., Yu, T., Zhu, L., Zhang, J., Wen, J., Gasc, J., Incel, S., Schubnel, A., Li, Z., Chen, T., Liu, W., Prakapenla, V., Jin, Z., 2018. Lower-crustal earthquakes in southern tibet are linked to eclogitization of dry metastable granulite. Nature communications 9, 1–13. doi:https://doi.org/10.1038/s41467-018-05964-1.

Shmonov, V., Vitiovtova, V., Zharikov, A., Grafchikov, A., 2003. Permeability of the continental crust: implications of experimental data. Journal of Geochemical Exploration 78, 697–699. doi:https://doi.org/10.1016/S0375-6742(03)00129-8.

Taetz, S., John, T., Bröcker, M., Spandler, C., Stracke, A., 2018. Fast intraslab fluid-flow events linked to pulses of high pore fluid pressure at the subducted plate interface. Earth and Planetary Science Letters 482, 33–43. doi:https://doi.org/10.1016/j.epsl.2017.10.044.

Turcotte, D.L., Schubert, G., 2002. Geodynamics. Cambridge university press. doi:https://doi.org/10.1017/CBO9780511843877.

Viete, D.R., Hacker, B.R., Allen, M.B., Seward, G.G., Tobin, M.J., Kelley, C.S., Cinque, G., Duckworth, A.R., 2018. Metamorphic records of multiple seismic cycles during subduction. Science advances 4, eaaq0234. doi:https://doi.org/10.1126/sciadv.aaq0234.

Vrijmoed, J.C., Podladchikov, Y.Y., Andersen, T.B., Hartz, E.H., 2009. An alternative model for ultra-high pressure in the svartberget fe-ti garnet-peridotite, western gneiss region, norway. Eu-

ropean Journal of Mineralogy 21, 1119–1133. doi:https://doi.org/10.1127/0935-1221/2009/0021-1985.

Yamato, P., Duretz, T., Angiboust, S., 2019. Brittle/ductile deformation of eclogites: insights from numerical models. Geochemistry, Geophysics, Geosystems 20, 3116–3133. doi:https://doi.org/10.1029/2019GC008249.

Yamato, P., Duretz, T., Baïsset, M., Luisier, C., 2022. Reaction-induced volume change triggers brittle failure at eclogite facies conditions. Earth and Planetary Science Letters 584, 117520. doi:https://doi.org/10.1016/j.epsl.2022.117520.

Zertani, S., John, T., Brachmann, C., Vrijmoed, J.C., Plümper, O., 2022. Reactive fluid flow guided by grain-scale equilibrium reactions during eclogitization of dry crustal rocks. Contributions to Mineralogy and Petrology 177, 61. doi:https://doi.org/10.1007/s00410-022-01928-3.

Zertani, S., Labrousse, L., John, T., Andersen, T.B., Tilmann, F., 2019. The interplay of eclogitization and deformation during deep burial of the lower continental crust—a case study from the bergen arcs (western norway). Tectonics 38, 898–915. doi:https://doi.org/10.1029/2018TC005297.